Characterization of Electrical Crosstalk in 4T-APS Arrays using TCAD Simulations

Juan Manuel López-Martínez, Ricardo Carmona-Galán and Ángel Rodríguez-Vázquez
Instituto de Microelectrónica de Sevilla-CNM
CSIC-Universidad de Sevilla
Sevilla, Spain
jmlopez@imse-cnm.csic.es

***Abstract*—TCAD simulations have been conducted on a CMOS image sensor in order to characterize the electrical component of the crosstalk between pixels through the study of the electric field distribution. The image sensor consists on a linear array of five pinned photodiodes (PPD) with their transmission gates, floating diffusion and reset transistors. The effect of the variations of the thickness of the epitaxial layer has been addressed as well. In fact, the depth of the boundary of the epitaxial layer affects quantum efficiency (QE) so a correlation with crosstalk has been identified.**

Keywords—CMOS; CMOS image sensors (CIS); active pixel sensor (APS); pinned photodiode (PPD); crosstalk; epitaxial layer; TCAD simulation.

I. INTRODUCTION

CMOS image sensors (CIS) based on pinned photodiodes (PPD) are widely used nowadays in consumer electronics as well as in high-end applications. This is mainly due to their advantages regarding low dark current and noise [1]-[3]. In the last years, efforts have been made to better understand key electrical properties of PPDs, like full well capacity, photodiode's capacitance or pinning voltage [4]-[10]. However, although crosstalk characterization has been since long considered an important source of sensitivity degradation and assessed for CCDs [2] and some CMOS devices [11], [12], studies on crosstalk on CMOS 4T-APS pixels have not been adequately addressed. Among other reasons, this may be due to the fact that CIS technology parameters are commonly unavailable. This makes it difficult to approach this problem by using TCAD simulations. Another problem is the computational cost; e.g., a five pixel linear array, like the one presented in this paper, already introduce long periods of computing due to the complexity of the structure.

Crosstalk (CTK) occurs when the charge generated by photon incident on a pixel are finally sensed by a neighboring pixel. CTK degrades performance of image sensor arrays. It also cuts down spatial resolution by blurring the sharp edges. Other detrimental effects are the reduction of the overall sensitivity, the degradation of the color separation, and the increase of image noise. Crosstalk is defined as the percentage of the total charge generated by incident light that is diverted to not-illuminated pixels in the neighborhood. There are two components for CTK. The optical crosstalk is related to illumination, reflection, refraction and scattering of photons in the different layers of the material that cover the photodiode. This generates stray photons that are absorbed in the neighborhood. The second component is electrical, and it involves the diffusion of photo-generated carriers between adjacent devices. This paper addresses the characterization of CTK in 4T-APS using TCAD tools. Particularly, the CTK relation with quantum efficiency (QE) will be explored and linked to the thickness —and thus the depth— of the epitaxial layer, a key parameter of the structure that affects both, CTK and QE. [13].

II. TCAD SIMULATION

A. Simulated devices

TCAD simulations have been conducted using Silvaco TCAD tools. All simulations have been defined over a 2D description of the structures for simplicity. The basic device structure and the pixel array are shown in Fig. 1. Each of the pixels of the array includes a PPD with its transfer gate (TG), a floating diffusion (FD) and a reset transistor (RST) allowing resetting the floating diffusion voltage to a reset value. The PPD includes the usual layers:

- The buried n-well (NW) and the P+ pinning implantations.
- The p-well (PW) that isolates the circuitry from the bulk.
- N+ boxes, used for floating diffusion and the drain of the reset transistor.
- A TG threshold adjustment layer.

The device fabrication process flow has been simulated with Athena, SSuprem4 and Elite tools, belonging to the set of Silvaco TCAD tools. All doping profiles were obtained from the dose info provided by [3]. Additional doping profiles for the PW and the p-substrate were used.

The resulting device have about 75,000 nodes [14] and a single simulation run with Atlas takes about 85 hours of simulation time with a 4-core processor, which gives an idea of its complexity.

B. Simulated tests

The device process simulations have been run with Atlas as part of Silvaco TCAD tools. The models used were [14]:

1) *CONSHR:* Concentration dependent carrier lifetimes.
2) *CVT:* Lombardi (CVT) model.
3) *FERMI:* Fermi-Dirac statistical model.

978-1-5090-6508-0/17/$31.00 ©2017 IEEE

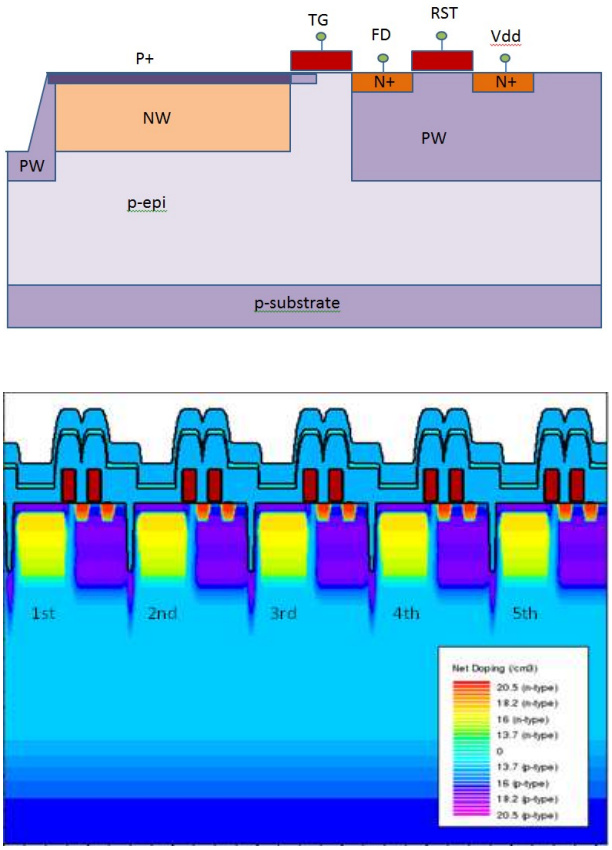

Fig. 1 Pixel cross-section (above) and pixel array doping profile, with the PPD numbered (bottom).

To characterize the crosstalk, we have employed a spot-scanning technique. It consists of, first, illuminating an individual pixel inside an array, and then measuring its effects in adjacent pixels. The crosstalk is defined as

$$CTK(\%) = \frac{I_0}{I_T} \cdot 100 \qquad (1)$$

where I_0 is the total current induced by stray carriers in the adjacent pixels when the central pixel is illuminated, and I_T is the total photo-generated current. Both are measured as the slopes of the generated charges against a fixed transient time [15].

Concerning the optical transmission, we will consider that the whole array is masked, except the central pixel active area, as we want to evaluate the electrical component of the crosstalk separately. Hence, the optical transmission is zero.

Therefore, we have considered a linear array of five pixels in which the central pixel is the only one to be illuminated at a fixed intensity of $1.4 \cdot 10^{-2}$ W/cm^2, so that the photodiode does not saturate in the integration time, and an illumination window of 1.45 µm that match that of the active area. We have measured the charge stored in the buried NW of the five pixels at a fixed luminous intensity and exposition time when they are reverse biased, so we can evaluate the photocurrent available on the non-illuminated pixels against the central one.

C. *Quantum efficiency and epitaxial layer thickness*

A key factor to be taken into account is the thickness of the p-epitaxial layer (ELT). As stated in [13], there is a quantifiable QE degradation when the p-epitaxial layer thickness decreases. This is because minority carriers generated in this layer are efficiently collected in the buried NW of the pixel, due to the high electric field established between the substrate and the well when the pixel is reverse biased. Also, the low concentration of impurities reduces the recombination rate of photo-generated carriers, thus increasing the diffusion length. When this layer is thinner, the substrate is closer to the surface. Minority carriers in the substrate are more likely to recombine due to a high impurity concentration, not reaching the high-field area. Therefore, QE degrades at longer wavelengths because these photons are absorbed at greater depths. This can be seen in Fig. 2. Shorter wavelengths, like is 410 and 474 nm in the graph, do not seem to suffer from this effect. Therefore, the longer the wavelength the larger the loss of QE.

D. *Crosstalk and epitaxial layer thickness*

ELT also affects CTK. To fully understand this effect, we have to study the electric fields within the bulk to be able to know how carrier motion is established. TCAD simulations allow us to measure both the module and the direction of the electric field. Also CTK can be visualized as electron current density between the second and third pixels. As shown in Fig. 3, three different regions between the depletion regions of two adjacent pixels can be clearly identified when the epitaxial layer is thinner. The first one is at the edge of the substrate and it will be labelled as border region (B). The second is characterized by opposing electric fields that create a potential valley where minority carriers can only diffuse between depletion regions, and thus will be labelled as valley region (V). Finally there is a strip of a relatively strong

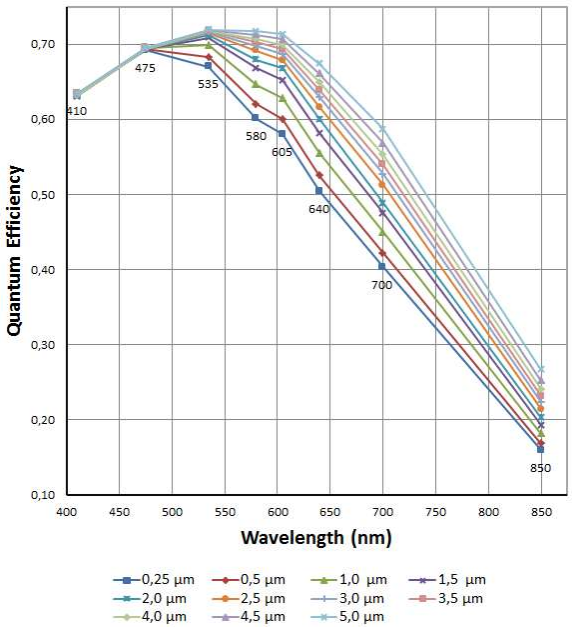

Fig. 2. Quantum efficiency vs. wavelength for several ELT.

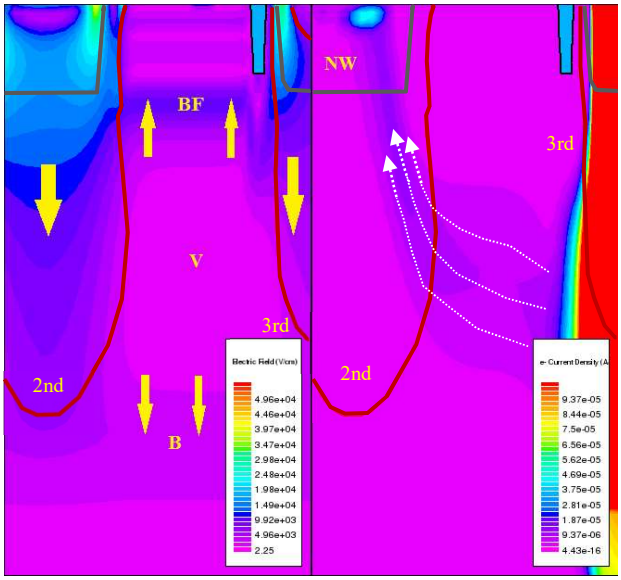

Fig. 3. Crosstalk between 2nd and 3rd pixels with ELT at 1,5 µm. Electric field is represented in the left graph. General electric field vector arrows are depicted. Electron current density is shown in the right graph. The red lines represent the depletion region edge and the grey ones the junctions.

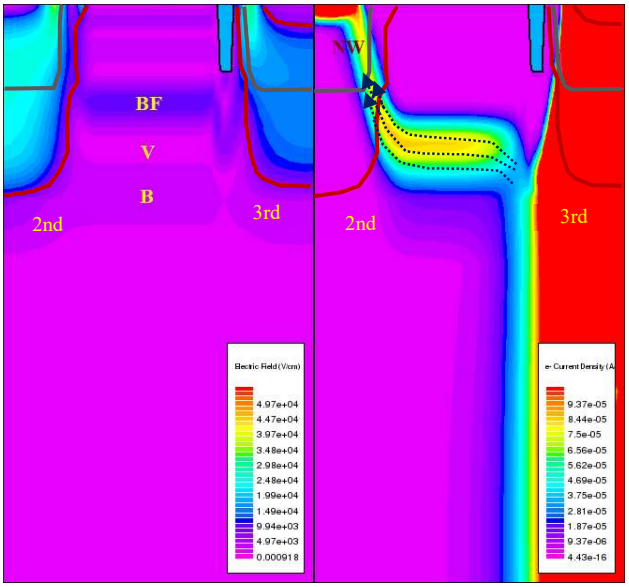

Fig. 4. Crosstalk between 2nd and 3rd pixels with ELT at 0.5 µm.

electric field between V and the PW, which will be the buffer region (BF). In B the electric field is not very strong, but is high enough to make minority carriers drift into V. As in B, the BF electric field conduct minority carriers towards the substrate and into V. In this region, the opposing electric fields allow the carriers to move freely. Some of these carriers can get through and reach the second pixel depletion region. Then, the minority carriers are collected in the buried NW, and thus the CTK occurs. As in the previous case, minority carriers that travel through V and reach the 4th pixel depletion region will be collected and measured as CTK. In this occasion however there is small potential barrier at the end of the V region due to the trench, that prevents many minority carriers in free diffusion to reach the depletion region, and thus CTK is considerably lower. Notice that in our simulations, 1st and 5th pixels registered meaningful CTK values only at shorts ELTs and longer wavelengths, but even then they were under 0.5%.

On the one hand, when ELT decreases, the V region becomes thinner, therefore reducing the volume where minority carriers may diffuse, and thus effectively increasing current density in this zone. This cause minority carrier velocity, and consequently diffusion length, to rise in V. Now carriers, which would have been recombined before, are able to reach the adjacent pixels, leading to CTK increase as shown in Fig. 4. On the other hand, when ELT increases from certain point on, B regions between pixels disappears. This happens when ELT is greater than the reach of the depletion region edge, and allows the photo-generated carriers to diffuse freely across the p-epitaxial layer into any of the pixels. If the rise of photo-generated carriers from the QE boost is also taken into account, is easy to see the CTK increase with ELT. This effect can be seen in Fig. 5. Total CTK, defined as the arithmetic sum of all adjacent pixels CTK, against wavelength for several ELT is shown in Fig. 6. As can be seen CTK increases with wavelength as shown in other works [2], [15]. Nevertheless the total CTK clearly expresses the dependence of the ELT.

The CTK values obtained are at their lowest in a range of 2.5 and 3 µm of ELT, when they reach the 4% for a wavelength of 850 nm. These values are low and in line with that of current literature [15]. However estimated CTK values can exceed the 10% if ELT is too large or even 15% if too reduced.

E. Crosstalk and quantum efficiency correlation

In order to find an optimal QE-CTK balance, it is in our interest to identify the best ELT for a desired wavelength range. This was analyzed by means of a study of the correlation between QE —and thus responsivity—, CTK and ELT. Fig. 7 shows the results obtained. The red dashed lines represent the correlation between QE and CTK when the epitaxial layer is thinner. This correlation is stronger when ELT decreases. Solid green lanes show the correlation between QE and CTK when the epitaxial layer is thicker. Here, CTK is greater at high QE because

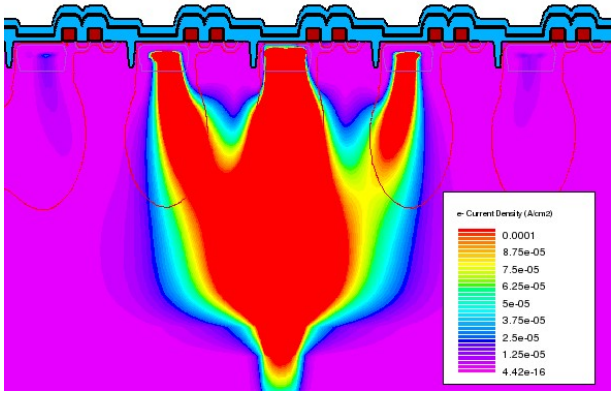

Fig. 5. Crosstalk representation as electron current density with ELT at 5 µm. In this graph, maximum electron current density is cut by 2 orders of magnitude so crosstalk in 1st and 5th pixels can be visualized.

minority carriers are allowed to move freely through the epitaxial layer. The blue dashed line represents the change in trend from a thinner epitaxial layer to a thicker one.

III. Conclusion

TCAD simulations have been used to shed some light on the crosstalk behavior in PPD arrays, including the increase of CTK with wavelength and its dependency with ELT. Besides, the CTK results obtained are good even at longer wavelengths in a fixed ELT range. Also the CTK correlation with QE has been shown, and while QE in NIR is low, the use of PPD for this range should be explored. These results show that choosing an adequate ELT is crucial to adjust the balance between CTK and QE, and maximize the pixel capabilities for a desired wavelength.

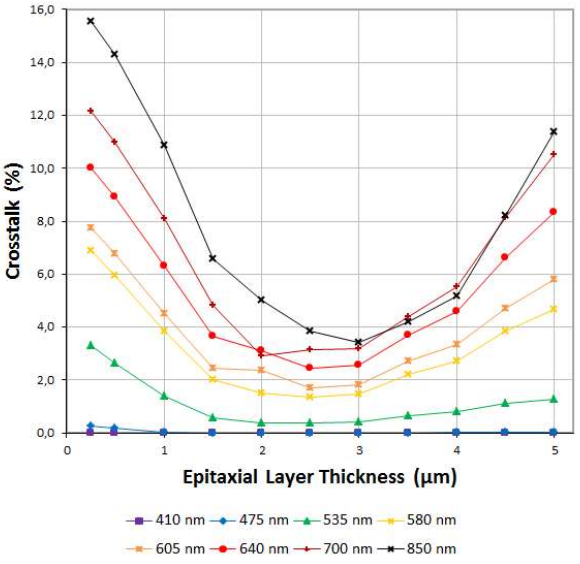

Fig. 6. Total crosstalk vs. ELT for several wavelengths.

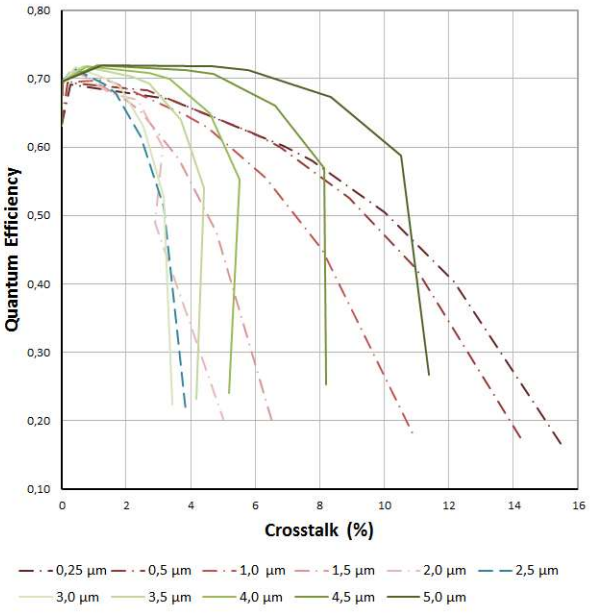

Fig. 7. Quantum efficiency vs. crosstalk for several ELT.

The results obtained show that TCAD simulations can be a good tool to characterize crosstalk. The main downside is the computational cost, which makes simulations of larger arrays inviable. Future work should be aimed to find ways to extrapolate crosstalk models from TCAD simulations to larger 4T-APS arrays, also do further research on structural changes on the array like pixel size and PPD geometry and how crosstalk affect final image sensor characteristics, like spatial responsivity and MTF.

Acknowledgement

This work was funded by the Spanish MINECO under project TEC2015-66878-C3-1-R (co-funded by ERDF-FEDER), by Junta de Andalucía's CEICE under grant TIC 2012-2338, and by ONR under grant N000141410355.

References

[1] N. Teranishi et al., "No image lag photodiode structure in the interline CCD image sensor," in *IEDM Tech. Dig*., vol. 28. 1982, pp. 324–327.

[2] B.C.Burkey et al., "The pinned photodiode for an interline-transfer CCD image sensor," in *IEDM Tech. Dig.*, vol. 30. Dec. 1984, pp. 28–31.

[3] E. R. Fossum and D. B. Hondongwa, "A review of the pinned photodiode for CCD and CMOS image sensors," *IEEE J. Electron Devices Soc.*, vol. 2, no. 3, pp. 33–43, May 2014.

[4] A. Krymski and K. Feklistov, "Estimates for scaling of pinned photodiodes," in *Proc. IEEE Workshop CCD Adv. Image Sensors*, Jun. 2005, pp. 60–63.

[5] S. Park and H. Uh, "The effect of size on photodiode pinch-off voltage for small pixel CMOS image sensors," *Microelectron. J.*, vol. 40, no. 1, pp. 137–140, Jan. 2009.

[6] C. Y.-P. Chao et al., "Extraction and estimation of pinned photodiode capacitance in CMOS image sensors," *IEEE J. Electron Devices Soc*., vol. 2, no. 4, pp. 59–64, Jul. 2014.

[7] V. Goiffon et al., "Pixel level characterization of pinned photodiode and transfer gate physical parameters in CMOS image sensors," *IEEE J. Electron Devices Soc.*, vol. 2, no. 4, pp. 65–76, Jul. 2014.

[8] A. Pelamatti et al., "Estimation and Modeling of the Full Well Capacity in Pinned Photodiode CMOS Image Sensors." *IEEE Electron Device Lett.*, vol. 34, no. 7, pp 900-902, Jul. 2013.

[9] A. Pelamatti et al., "Temperature dependence and dynamic behavior of full well capacity in pinned photodiode CMOS image sensors," *IEEE Trans. Electron Devices*, vol. 62, no. 4, pp. 1200–1207, Apr. 2015.

[10] C. Cao et al., "An improved model for the full well capacity in pinned photodiode CMOS image sensors," *IEEE J. Electron Devices Soc*., vol. 4, no. 3, pp. 306–310, Jul. 2015.

[11] I. Brouk et al., "Characterization of crosstalk between CMOS photodiodes," *Solid-State Electron.*, vol. 46, no. 1, pp. 53–59, 2002.

[12] G. Agranov et al., "Crosstalk and microlens study in a color CMOS image sensor," *IEEE Trans. Electron Devices*, vol. 50, no. 1, pp. 4–11, Jan. 2003.

[13] G. Agranov et al., "Super small, sub 2 µm pixels for novel CMOS image sensors," in *Proc. Int. Image Sensor Workshop 2007*, pp. 307–310.

[14] *Atlas User's Manual: Device Simulation Software*. Silvaco Inc., Santa Clara, CA, 2016.

[15] M. Estribeau and P. Magnan, "Pixel Crosstalk and Correlation with Modulation Transfer Function of CMOS Image Sensor," in *Proc. SPIE* vol. 5677, pp. 98-108, Mar. 2005.